Journal of Materials Chemistry C

PAPER

View Article Online
View Journal | View Issue

Cite this: J. Mater. Chem. C, 2019, 7, 12306

Predicted polymorph manipulation in an exotic double perovskite oxide†

He-Ping Su,[a] Shu-Fang Li,*[b] Yifeng Han,[b] Mei-Xia Wu,[b] Churen Gui,[c] Yanfen Chang,[d] Mark Croft,[e] Steven Ehrlich,[f] Syed Khalid,[f] Umut Adem,[g] Shuai Dong,[c] Young Sun,[d] Feng Huang[h] and Man-Rong Li*[b]

Received 22nd June 2019,
Accepted 10th September 2019

DOI: 10.1039/c9tc03367j

rsc.li/materials-c

Predicted polymorph manipulation offers a cutting-edge route to design function-oriented materials in an exotic double perovskite-related oxide $A_2BB'O_6$ with small A-site cations. Herein, first-principles density functional theory calculations in light of the equation of state for solid, for the first time, was used to predict the Mg_3TeO_6 ($R\bar{3}$)-to-perovskite ($P2_1/n$) type phase transition in Mn_3TeO_6 at around 5 GPa, regardless of the deployment of magnetic interactions. The high-pressure synthesis and synchrotron diffraction crystal structure analysis corroborated experimentally the polymorph variation in $Mn_2^{2+}Mn^{2+}Te^{6+}O_6$, which was accompanied by a 13 K increase in the antiferromagnetic ordering temperature (37 K) in the high-pressure perovskite polymorph compared to that of the ambient-pressure $R\bar{3}$ phase (24 K). The magnetodielectric coupling remains up to 50 K with the maximum being around the magnetic ordering temperature in the perovskite Mn_3TeO_6. Thus, the predicted polymorph manipulation here offers the possibility of discovering accelerated materials by inverse design in exotic perovskite oxides.

Pressure-driven polymorph evolution is a pre-eminent strategy for property-oriented material design,[1,2] as it has been extensively applied to achieve the desired function in an exotic perovskite-related ABO_3 and $A_2BB'O_6$ oxides with small A-site cations.[3–11] For example, the multiferroic $LiNbO_3$-type ($R3c$) $ScFeO_3$ and $FeTiO_3$ can be achieved at 6 and 12 GPa from their ambient-pressure (AP) bixbyite ($Ia\bar{3}$) and ilmenite ($R\bar{3}$) precursors, respectively,[3,4,6] and the perovskite ($Pnma$) polymorph of $MnVO_3$ (a type-II multiferroics) can be synthesized from its lower-pressure (3 GPa) ilmenite analog above 5 GPa.[7] Practical magnetoelectricity has also been discovered in compounds with enhanced magnetic interactions in the transition-metal-only perovskite-related phases such as Mn_2FeMO_6 (M = Mo,[9] Re[10,11]) prepared at high pressure (HP). However, so far, the pressure-dependent polymorph modification of the exotic perovskites is still a high-cost and low-efficient trial-and-error process, largely due to their undistinguishable values of the geometrical descriptors like the perovskite-related tolerance factor (t).[12] Thus, there is not yet any universal rule to precisely govern or predict the polymorphs of a given composition. Recently, first-principles density functional theory (DFT) calculations of the total energy based on the equations of state[13,14] have shed light on the structure prediction of simple ABO_3 exotic perovskites, as proposed in the pressure-induced $LiSbO_3$-to-$LiNbO_3$ transition in $LiSbO_3$,[15] and ilmenite-perovskite-$LiNbO_3$ conversion in $ZnTiO_3$,[16] in which the calculated results established pressure-dependent phase stability maps of each polymorph candidate (ilmenite, perovskite, $LiNbO_3$, and $LiSbO_3$) for $LiSbO_3$ and $ZnTiO_3$, and well explained the experimentally observed phase evolution. These findings suggested the possible structure prediction of the exotic perovskite oxides by estimating the total energy of the polymorph candidate.

In the non-magnetic simple ABO_3-system, such as $LiSbO_3$ and $ZnTiO_3$, the image is more clear than in double $A_2BB'O_6$-system, where the increased diversity of the cationic arrangements yield six possible polymorphs, reported to date, namely, distorted $GdFeO_3$-type double perovskites ($P2_1/n$), B-site ordered $LiSbO_3$ derivatives ($Pnn2$), Mg_3TeO_6 ($R\bar{3}$), corundum derivatives (ordered ilmenite or Ni_3TeO_6 type $R3$), bixbyite ($Ia\bar{3}$), and β-Li_3VF_6 ($C2/c$) (Fig. 1). Further complexity also arises from the multi-dimensional competition in the magnetic $A_2BB'O_6$-system.[17] Thus, the ability to precisely predict and manipulate polymorphs requires the understanding of interplays between the macroscopic

[a] School of Physics, Sun Yat-Sen University, Guangzhou 510275, P. R. China
[b] Key Laboratory of Bioinorganic and Synthetic Chemistry of Ministry of Education, School of Chemistry, Sun Yat-Sen University, Guangzhou 510275, P. R. China
[c] School of Physics, Southeast University, Nanjing 211189, China
[d] Beijing National Laboratory for Condensed Matter Physics, Institute of Physics, Chinese Academy of Sciences, Beijing 100190, P. R. China
[e] Department of Physics and Astronomy, Rutgers, The State University of New Jersey, Piscataway, NJ 08854, USA
[f] NSLS-II, Brookhaven National Laboratory, Upton, NY 11973, USA
[g] Department of Materials Science and Engineering, İzmir Institute of Technology, Urla 35430, İzmir, Turkey
[h] School of Materials, Sun Yat-Sen University, Guangzhou 510275, P. R. China. E-mail: limanrong@mail.sysu.edu.cn

† Electronic supplementary information (ESI) available. CCDC 1912424 and 1912425. For ESI and crystallographic data in CIF or other electronic format see DOI: 10.1039/c9tc03367j

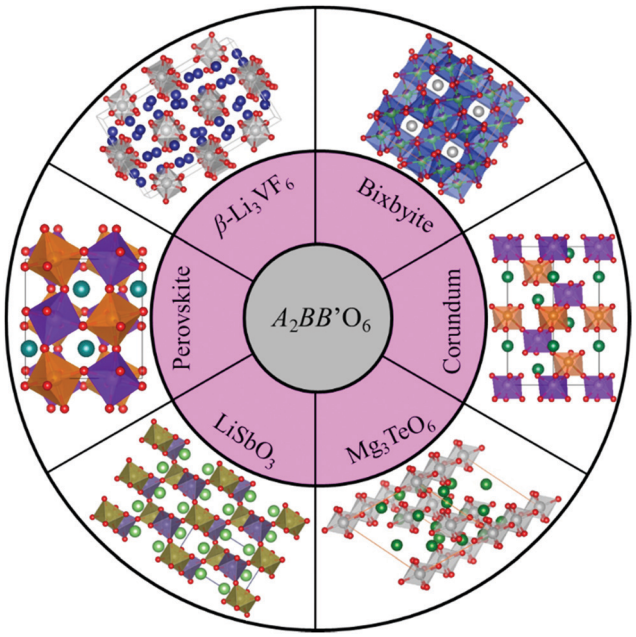

Fig. 1 Possible crystal structure types of $A_2BB'O_6$ with small A site cations, including distorted $GdFeO_3$-type double perovskites ($P2_1/n$), B-site ordered $LiSbO_3$ derivatives ($Pnn2$), Mg_3TeO_6 ($R\bar{3}$), corundum derivatives ($LiNbO_3$-type $R3c$, ilmenite $R\bar{3}$, and ordered ilmenite or Ni_3TeO_6 type $R3$), bixbyite ($Ia\bar{3}$), and β-Li_3VF_6 ($C2/c$).

(synthesis conditions) and microscopic (electronic spin, charge, orbital structures, and lattice) factors. To the best of our knowledge, so far, no such research work has been reported with regards to the use of magnetically active exotic double perovskite-related $A_2BB'O_6$ compounds to elucidate the contribution of magnetic interactions in the polymorph prediction.

In this work, we present for the first time the predicted polymorph manipulation in exotic double perovskite-related Mn_3TeO_6 (MTO), and studied its crystal structure evolution and the accompanied physical property variation.

AP-prepared A_3TeO_6 showed very similar t, but adopted four possible structural types (Fig. 1): Mg_3TeO_6-type ($R\bar{3}$) for A = Mg (t = 0.822)[18] and Mn (t = 0.836);[19] β-Li_3VF_6-type ($C2/c$) for A = Co (t = 0.822)[20] and Zn (t = 0.823);[21] polar corundum ($R3$) in Ni_3TeO_6 (t = 0.819);[22] and bixbyite in Cu_3TeO_6 (t = 0.816),[23] providing an ideal platform to understand the polymorph modification. The AP-MTO was found to be isostructural with the rhombohedral ($R\bar{3}$) Mg_3TeO_6, as illustrated in Fig. S1 and S2 (ESI†), which displays the antiferromagnetic (AFM) type-II multiferroic behavior.[24] To investigate the structure variation of MTO under pressure, the first-principles DFT calculations, in light of the equation of state for solid, were conducted in three most probable polymorphs, namely, $R\bar{3}$ (AP-MTO in Mg_3TeO_6), $R3$ (polar corundum Ni_3TeO_6-type), and $P2_1/n$ (distorted $GdFeO_3$-type perovskite). Chemically and geometrically, the size and charge difference between Mn^{2+} (the ionic radius in octahedral(VI) coordination ^{VI}r = 0.83 Å) and Te^{6+} (^{VI}r = 0.56 Å) energetically did not favor the formation of bixbyite $Ia\bar{3}$, $LiSbO_3$-derived $Pnn2$, or β-Li_3VF_6-type $C2/c$ (Section 2.2 of ESI†), and thus, they were not considered in the calculations.

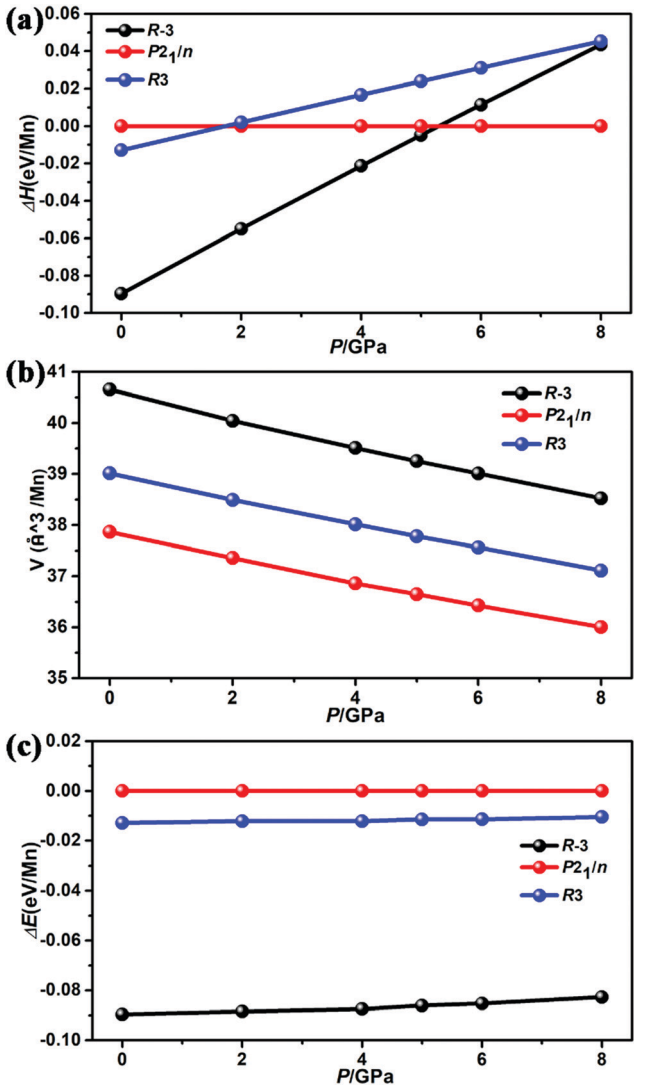

Fig. 2 The pressure dependencies of the relative enthalpies (a), volume (b), and energy (c) for Mg_3TeO_6 ($R\bar{3}$), double perovskite ($P2_1/n$), and polar corundum ($R3$) types of Mn_3TeO_6.

Fig. 2 shows the variation of relative enthalpies, volume, and total energy for the three types of MTO phases.[13] Further, the enthalpy of AP-MTO was observed to be the lowest under lower-pressure conditions, while the $P2_1/n$-type structure became more stable at higher pressure (Fig. 2a). Moreover, the volume of $P2_1/n$-type HP-MTO was estimated to be the smallest under pressure (Fig. 2b). The phase transition, which occurred at ~5 GPa indicated that the $R3$-type MTO was less stable than the $P2_1/n$-type HP-MTO, and hence the AP-MTO can directly transform into $P2_1/n$-type HP-MTO.

This conversion pressure of ~5 GPa coincided well with the experimental results, as the synthesis at 5 GPa yielded a $P2_1$/n-type polymorph. Obviously, the polar $R3$ state does not appear throughout the whole calculations from the energic point of view. Therefore, the quantitative results (the ΔH or the critical pressure shown in Fig. 2a) could change slightly with various calculation parameters, such as the Coulomb repulsion U

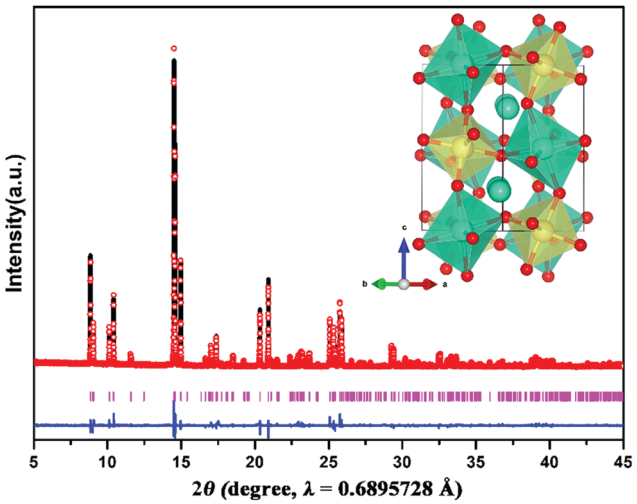

Fig. 3 Rietveld refinements from the SPXD data of HP-MTO prepared at 5 GPa and 1173 K in $GdFeO_3$-type distorted monoclinic structure ($P2_1/n$). Inset shows the perspective polyhedral view of the unit cell structure along *c* direction. Mn_2O_6, green; TeO_6, yellow; Mn1, green spheres; and O, red spheres.

(Table S1, ESI†), but the overall qualitative trends in the structure were steady. Additionally, the effect of Dzyaloshinskii–Moriya (DM) interaction for different proposed ferromagnetic/antiferromagnetic (FM/AFM) spin structures did not confound the overall results; therefore, in order to focus on the pressure effect on the structure, the simplest FM order was adopted in all calculations by ignoring the energy shift that complex magnetic orders may undergo.

The HP-MTO polymorph was observed to adopt a typical monoclinic ($P2_1/n$) double perovskite structure, synthesized at 5 GPa between 1173–1273 K, following the prediction in Fig. 2, with subsequent refinement using the SPXD data, as shown in Fig. 3. Attempts to synthesize the HP-MTO phase below 5 GPa/1173 K were unsuccessful and yielded either the AP phase or a mixture of both polymorphs (Fig. S3, ESI†). Moreover, the dense polycrystalline pellets and small single crystals ($\sim$20 μm) of the HP phase can be obtained at 1173 and 1273 K, respectively, which presented the identical PXD patterns. Therefore, the detailed crystal structure analyses were conducted using both powder and single-crystal diffraction methods. The final refined crystallographic parameters and agreement factors are listed in Table S2 (ESI†). Additionally, the selected interatomic distances, bond angles, and bond valence sum (BVS) calculations are listed in Table S3 (ESI†).

Because the crystallographic data from SPXD and single-crystal diffraction approaches were almost identical within the estimated standard deviation, the results from SPXD in Tables S2 and S3 (ESI†) were used to discuss the crystal structure of HP-MTO, given the higher resolution of synchrotron beamline. The crystal structure of HP-MTO ($P2_1/n$) (No. 14), in which a = 5.2945(1) Å, b = 5.4527(1) Å, c = 7.8092(1) Å, β = 90.37(1)°, V = 225.44 (1) Å^3, Z = 2, R_{wp} = 9.96%, and R_p = 6.50%, is shown in the inset of Fig. 3, and is isostructural with other $Mn_2BB'O_6$ double perovskites.[10,11,25–33] It was also observed that the structure consisted of $Mn1O_8$ coordination and rock-salt ordering of Mn_2O_6 and TeO_6 octahedra. The average ⟨Mn1–O⟩ bond length (2.425(1) Å) was in line with those of the A-site ⟨Mn–O⟩ in isostructural $Mn_2BB'O_6$ varying between 2.379 and 2.406 Å.[10,26,29,33] The ⟨Mn2–O⟩ of 2.175(1) Å was somewhat longer than that of the B-site $Mn^{2+/3+}$ (2.138(1) Å) in the isostructural Mn_2MnReO_6,[28] which was reasonable upon considering the ionic size difference between Mn^{2+} and Mn^{3+}.[34] The TeO_6 octahedron was found to be more regular with the Te–O distance between 1.916(1) and 1.967(1) Å. Comparison of the structural parameters with the parent analogs suggested formal oxidation states of $Mn_2^{2+}Mn^{2+}Te^{6+}O_6$ of the HP perovskite polymorph, as further corroborated by the BVS calculations (Table S3, ESI†) and XANES analysis discussed in Fig. S4 and Section 2.1 of ESI.†

The HP synthesis could enhance the steric atomic interactions and induce transformation to denser structures with higher internal energy (Fig. 2c) related to the thermodynamic stability.[35–37] When heated at AP, an HP-phase can either decompose or revert back to the AP-phase. For example, the recently reported $LiSbO_3$-derived HP-Li_2GeTeO_6 (orthorhombic *Pnn*2, prepared at 3–5 GPa and 1073 K) can persist up to 843 K at AP before fully converting back to the AP-ordered ilmenite (*R*3) analog, accompanied by cell volume expansion and decreasing density from 5.23 to 4.97 g cm^{-1}.[37] Similarly, the perovskite polymorph of Mn_2CrSbO_6 ($P2_1/n$, prepared at 8 GPa and 1473 K) underwent a phase transition to ilmenite ($R\bar{3}$) after thermal treatment at 973 K.[27] Fig. 4 presents the room-temperature PXD patterns of the HP-MTO (5 GPa and 1273 K product) after annealing at variable temperatures. It can be seen that the $P2_1/n$ phase persisted up to 823 K, and converted back to the AP-MTO above 873 K.

The temperature-dependent susceptibilities for HP-MTO measured in the field of H = 1000 Oe are shown in Fig. 5a.

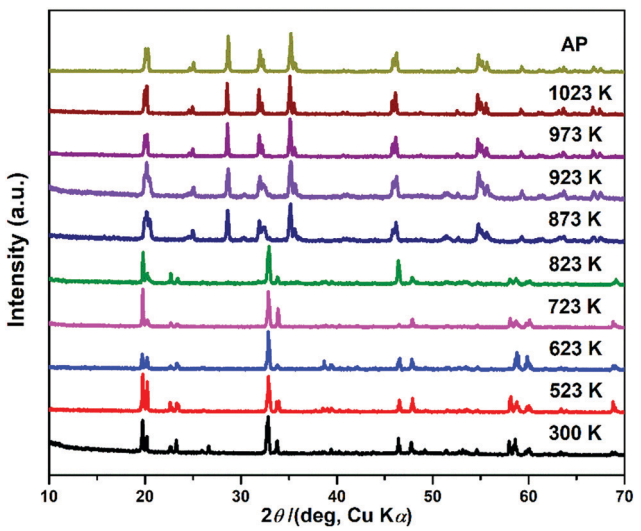

Fig. 4 Room-temperature PXD patterns of HP-MTO after annealing it from 300 to 1023 K in Ar for 30 min at each temperature point. The PXD patterns of the AP-MTO are plotted on the top for comparison. The relative intensity variation of the patterns after being annealed in the temperature range of 300–873 K, owing to the preferred orientation.

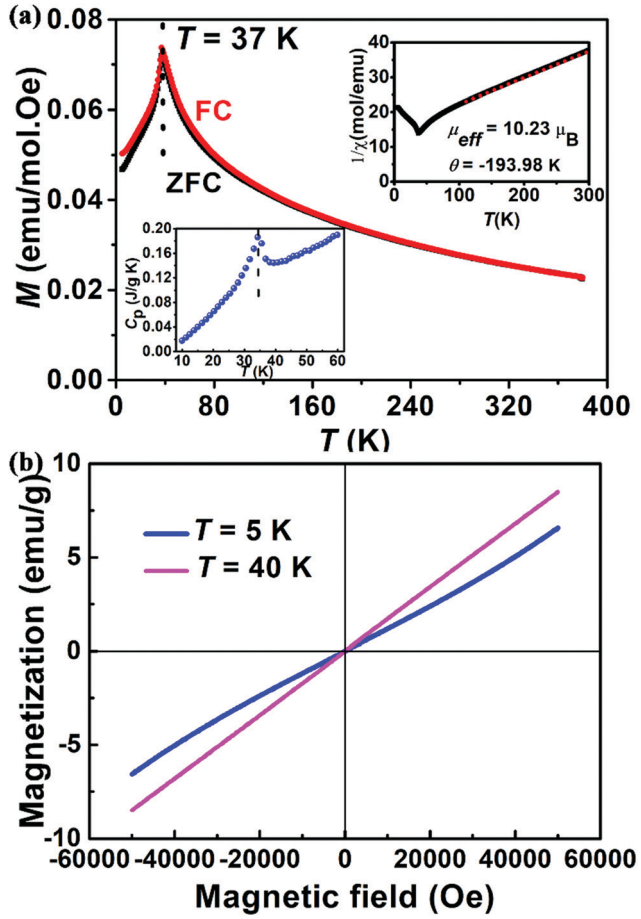

Fig. 5 (a) The temperature-dependent susceptibility and (inset) inverse susceptibility of the HP-MTO measured from 5 K to 380 K under magnetic field of 1000 Oe. (b) Isothermal magnetization measured at 5 and 40 K, respectively.

The ZFC (zero-field cooling) and FC (field cooling) curves exhibited typical AFM behavior with Néel temperature T_N of 37 K. The Curie–Weiss (CW) temperature θ_{CW} from the fit to $\chi(T) = C/(T - \theta_{CW})$ converged to −193.98 K, indicating that the interactions in HP-MTO were dominated by AFM, as further evidenced by the isothermal $M(H)$ curves in Fig. 5b. Furthermore, the effective magnetic moment μ_{eff} of 10.23 μ_B f.u.$^{-1}$ (formula unit) indicated a $S = 5/2$ high-spin state of Mn^{2+} ($\mu_{eff}(Mn^{2+}) \sim 5.89\ \mu_B$) as evidenced by the crystal structure and XANES results. For temperatures below about 130 K, the $\chi(T)$ deviated clearly from the CW behavior, suggesting that the short-range correlations started to develop, as manifested by the slightly indicative hysteresis in Fig. 5b. Compared with the AP-MTO (AFM ordering below 24 K),[38] the HP-MTO becomes ordered at a higher temperature, as suggested by the sharp peak at 37 K in Fig. 5a.

At low temperatures, a relatively sharp peak was observed at 34.9 K in the heat capacity curve, as shown in the inset of Fig. 5a, which echoes the AFM transition detected in the magnetic susceptibility measurements. This latter determination of the Néel temperature was more accurate than the magnetic measurements, as closer data points were recorded in the heat capacity measurements.

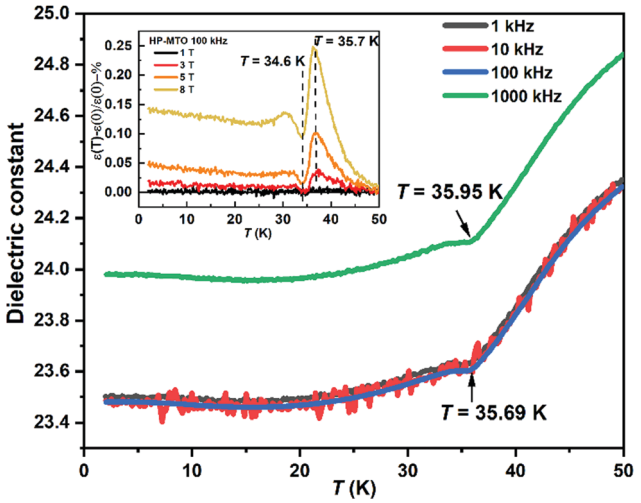

Fig. 6 Maximum magnetodielectric coupling occurs near the magnetic ordering temperature, with the magnetodielectric effects persisting up to about 50 K.

Temperature dependence of the dielectric constant for the HP-MTO sample showed an anomaly at T_N = 34.6 K (Fig. 6), whereas no anomaly could be detected in the temperature dependence of dielectric loss. This anomaly in ε around $T_N \sim$ 35.7 K demonstrated the presence of magnetodielectric coupling in HP-MTO. The temperature of this anomaly shifted with an increase in the frequency. Therefore, dielectric relaxation effects can be ruled out. At the highest measurement frequency of 1 MHz, the dielectric constant increased with respect to the measurements at lower frequencies. This kind of increase in the dielectric constant, at high frequencies, typically results from the inductive contribution of the measurement leads. However, this weak anomaly at T_N was not a divergent peak, suggesting the absence of ferroelectric order below T_N. In agreement with this conclusion, no detectable pyroelectric response was observed from the polycrystalline HP-MTO.

Apparently, the HP-MTO crystallized in a centrosymmetric space group $P2_1/n$, and unlike in the parent $R\bar{3}$ AP-MTO,[39] the magnetic order in HP-MTO was probably not cycloidal and/or helical, and does not induce ferroelectricity. Generally, the confirmation of the absence of ferroelectricity requires neutron diffraction experiments and further measurements on single-crystal samples, which are planned as future work. Application of the magnetic field slightly increased the dielectric constant and shifted the dielectric anomaly at the magnetic ordering temperature to slightly lower temperatures, as shown in the inset of Fig. 6. Additionally, the maximum magnetodielectric coupling occurred near the magnetic ordering temperature, and the magnetodielectric effect remained up to about 50 K.

Conclusions

In summary, the polymorph manipulation by the computational prediction of the relative energetics of competing phases has been, for the first time, observed in an exotic double

perovskite with small A-site cations. A pressure-induced Mg_3TeO_6 ($R\bar{3}$) to double perovskite ($P2_1/n$) type phase transition was predicted to occur around 5 GPa in Mn_3TeO_6, which was further manifested by an experimental synthesis and crystallographic analysis. This polymorph conversion was accompanied by about 15 K higher antiferromagnetic ordering temperature and magnetodielectric coupling in the perovskite phase. The predicted polymorph manipulation in Mn_3TeO_6, for the first time, builds a connection between Mg_3TeO_6 and double perovskite polymorphs, thus broadening the platform for structure modulation in $A_2BB'O_6$. It is also shown that the energetic effect of different magnetic structures may not be so critical in polymorph prediction in light of the equation of state for solids, as the energy contribution from the DM interaction does not dominate the ground states of the competing polymorphs. Thus, these findings will help to accelerate the discovery of new materials *via* data mining and high-throughput calculations in exotic $A_2BB'O_6$ (more than 13 000 new compounds by estimation under charge balance), and are of great interest for the in-depth study of magnetic materials or to access preparation methods and properties of multifunctional materials.

Conflicts of interest

There are no conflicts to declare.

Acknowledgements

This work was financially supported by the National Science Foundation of China (NSFC-21801253, 11804404, and 21875287). Work at Brookhaven National Laboratory was supported by the DOE BES (DE-SC0012704) on the NSLS-II Beamline 7BM and on NSLS-I on the X19A. The authors thank beamline BL14B1 (Shanghai Synchrotron Radiation Facility) for providing the beam time and helps during experiments. The authors would like to thank Prof. David Walker at LDEO in Columbia University for enlightening discussions.

Notes and references

1 Y. Hamasaki, T. Shimizu, S. Yasui, T. Taniyama, O. Sakata and M. Itoh, *Cryst. Growth Des.*, 2016, **16**, 5214–5222.
2 R. Ramesh and D. G. Schlom, *Nat. Rev. Mater.*, 2019, **4**, 257–268.
3 T. Kawamoto, K. Fujita, I. Yamada, T. Matoba, S. J. Kim, P. Gao, X. Pan, S. D. Findlay, C. Tassel, H. Kageyama, A. J. Studer, J. Hester, T. Irifune, H. Akamatsu and K. Tanaka, *J. Am. Chem. Soc.*, 2014, **136**, 15291–15299.
4 M.-R. Li, U. Adem, S. R. C. McMitchell, Z. Xu, C. I. Thomas, J. E. Warren, D. V. Giap, H. Niu, X. Wan, R. G. Palgrave, F. Schiffmann, F. Cora, B. Slater, T. L. Burnett, M. G. Cain, A. M. Abakumov, G. van Tendeloo, M. F. Thomas, M. J. Rosseinsky and J. B. Claridge, *J. Am. Chem. Soc.*, 2012, **134**, 3737–3747.
5 Y. Inaguma, M. Yoshida and T. Katsumata, *J. Am. Chem. Soc.*, 2008, **130**, 6704–6705.
6 T. Varga, A. Kumar, E. Vlahos, S. Denev, M. Park, S. Hong, T. Sanehira, Y. Wang, C. Fennie, S. Streiffer, X. Ke, P. Schiffer, V. Gopalan and J. Mitchell, *Phys. Rev. Lett.*, 2009, **103**, 047601.
7 M. Markkula, A. M. Arevalo-Lopez, A. Kusmartseva, J. A. Rodgers, C. Ritter, H. Wu and J. P. Attfield, *Phys. Rev. B: Condens. Matter Mater. Phys.*, 2011, **84**, 094450.
8 J. Cong, K. Zhai, Y. Chai, D. Shang, D. D. Khalyavin, R. D. Johnson, D. P. Kozlenko, S. E. Kichanov, A. M. Abakumov, A. A. Tsirlin, L. Dubrovinsky, X. Xu, Z. Sheng, S. V. Ovsyannikov and Y. Sun, *Nat. Commun.*, 2018, **9**, 2996.
9 M.-R. Li, M. Retuerto, D. Walker, T. Sarkar, P. W. Stephens, S. Mukherjee, T. S. Dasgupta, J. P. Hodges, M. Croft, C. P. Grams, J. Hemberger, J. Sánchez-Benítez, A. Huq, F. O. Saouma, J. I. Jang and M. Greenblatt, *Angew. Chem., Int. Ed.*, 2014, **53**, 10774–10778.
10 M.-R. Li, M. Retuerto, Z. Deng, P. W. Stephens, M. Croft, Q. Huang, H. Wu, X. Deng, G. Kotliar, J. Sánchez-Benítez, J. Hadermann, D. Walker and M. Greenblatt, *Angew. Chem., Int. Ed.*, 2015, **54**, 12069–12073.
11 A. M. Arévalo-López, G. M. McNally and J. P. Attfield, *Angew. Chem., Int. Ed.*, 2015, **54**, 12074–12077.
12 M. W. Lufaso and P. M. Woodward, *Acta Crystallogr., Sect. B: Struct. Sci.*, 2001, **57**, 725–738.
13 F. D. Murnaghan, *Proc. Natl. Acad. Sci. U. S. A.*, 1944, **30**, 244–247.
14 C. Collins, M. S. Dyer, A. Demont, P. A. Chater, M. F. Thomas, G. R. Darling, J. B. Claridge and M. J. Rosseinsky, *Chem. Sci.*, 2014, **5**, 1493–1505.
15 Y. Inaguma, A. Aimi, D. Mori, T. Katsumata, M. Ohtake, M. Nakayama and M. Yonemura, *Inorg. Chem.*, 2018, **57**, 15462–15473.
16 Y. Inaguma, A. Aimi, Y. Shirako, D. Sakurai, D. Mori, H. Kojitani, M. Akaogi and M. Nakayama, *J. Am. Chem. Soc.*, 2014, **136**, 2748–2756.
17 D. Yi, N. Lu, X. Chen, S. Shen and P. Yu, *J. Phys.: Condens. Matter*, 2017, **29**, 443004.
18 G. Blasse and W. Hordijk, *J. Solid State Chem.*, 1972, **5**, 395–397.
19 H. Singh, A. K. Sinha, H. Ghosh, M. N. Singh, P. Rajput, C. L. Prajapat, M. R. Singh and G. Ravikumar, *J. Appl. Phys.*, 2014, **116**, 074904.
20 H. Singh, H. Ghosh, T. V. Chandrasekhar Rao, G. Sharma, J. Saha and S. Patnaik, *J. Appl. Phys.*, 2016, **119**, 044104.
21 M. Weil, *Acta Crystallogr., Sect. E: Struct. Rep. Online*, 2006, **62**, i246–i247.
22 J. W. Kim, S. Artyukhin, E. D. Mun, M. Jaime, N. Harrison, A. Hansen, J. J. Yang, Y. S. Oh, D. Vanderbilt, V. S. Zapf and S. W. Cheong, *Phys. Rev. Lett.*, 2015, **115**, 137201.
23 X. Zhu, Z. Wang, X. Su and P. M. Vilarinho, *ACS Appl. Mater. Interfaces*, 2014, **6**, 11326–11332.
24 M. Weil, *Acta Crystallogr., Sect. E: Struct. Rep. Online*, 2006, **62**, i244–i245.
25 E. Solana-Madruga, A. J. Dos santos-Garcia, A. M. Arevalo-Lopez, D. Avila-Brande, C. Ritter, J. P. Attfield and R. Saez-Puche, *Dalton Trans.*, 2015, **44**, 20441–20448.

26 G. V. Bazuev, A. P. Tyutyunnik, M. V. Kuznetsov and Y. G. Zainulin, *J. Supercond. Novel Magn.*, 2018, **31**, 2907–2914.
27 A. J. Dos santos-Garcia, E. Solana-Madruga, C. Ritter, D. Avila-Brande, O. Fabelo and R. Saez-Puche, *Dalton Trans.*, 2015, **44**, 10665–10672.
28 A. M. Arevalo-Lopez, F. Stegemann and J. P. Attfield, *Chem. Commun.*, 2016, **52**, 5558–5560.
29 M.-R. Li, J. P. Hodges, M. Retuerto, Z. Deng, P. W. Stephens, M. C. Croft, X. Deng, G. Kotliar, J. Sánchez-Benítez, D. Walker and M. Greenblatt, *Chem. Mater.*, 2016, **28**, 3148–3158.
30 A. J. D. Santos-García, C. Ritter, E. Solana-Madruga and R. Sáez-Puche, *J. Phys.: Condens. Matter*, 2013, **25**, 206004.
31 R. Mathieu, S. A. Ivanov, I. V. Solovyev, G. V. Bazuev, P. Anil Kumar, P. Lazor and P. Nordblad, *Phys. Rev. B: Condens. Matter Mater. Phys.*, 2013, **87**, 014408.
32 A. P. Tyutyunnik, G. V. Bazuev, M. V. Kuznetsov and Y. G. Zainulin, *Mater. Res. Bull.*, 2011, **46**, 1247–1251.
33 M.-R. Li, P. W. Stephens, M. Croft, Z. Deng, W. Li, C. Jin, M. Retuerto, J. P. Hodges, C. E. Frank, M. Wu, D. Walker and M. Greenblatt, *Chem. Mater.*, 2018, **30**, 4508–4514.
34 R. Shannon, *Acta Crystallogr., Sect. A: Cryst. Phys., Diffr., Theor. Gen. Crystallogr.*, 1976, **32**, 751–767.
35 G. Liu, J. Gong, L. Kong, R. D. Schaller, Q. Hu, Z. Liu, S. Yan, W. Yang, C. C. Stoumpos, M. G. Kanatzidis, H.-K. Mao and T. Xu, *Proc. Natl. Acad. Sci. U. S. A.*, 2018, **115**, 8076.
36 Z. Gao, Y. Liu, C. Lu, Y. Xia, L. Fang, Y. Ma, Q. He, D. He and S. Yang, *J. Am. Ceram. Soc.*, 2018, **101**, 2571–2577.
37 M. H. Zhao, W. Wang, Y. Han, X. Xu, Z. Sheng, Y. Wang, M. Wu, C. P. Grams, J. Hemberger, D. Walker, M. Greenblatt and M. R. Li, *Inorg. Chem.*, 2019, **58**, 1599–1606.
38 R. Mathieu, S. A. Ivanov, P. Nordblad and M. Weil, *Eur. Phys. J. B*, 2013, **86**, 1–4.
39 L. Zhao, Z. Hu, C.-Y. Kuo, T.-W. Pi, M.-K. Wu, L. H. Tjeng and A. C. Komarek, *Phys. Status Solidi RRL*, 2015, **9**, 730–734.